International Journal of Multiphase Flow 35 (2009) 101–117

Contents lists available at ScienceDirect

International Journal of Multiphase Flow

journal homepage: www.elsevier.com/locate/ijmulflow

A vaporization model for discrete multi-component fuel sprays

Youngchul Ra *, Rolf D. Reitz

Engine Research Center, University of Wisconsin–Madison, 1500 Engineering Drive, ERB #1016B Madison, WI 53706, USA

ARTICLE INFO

Article history:
Received 14 July 2008
Received in revised form 14 October 2008
Accepted 20 October 2008
Available online 6 November 2008

ABSTRACT

A vaporization model for multi-component fuel sprays is described. The discrete multi-component (DMC) fuel approach was used to model the properties and composition of gasoline and diesel model fuels. Unsteady vaporization of single and multi-component fuel droplets and sprays was considered for both normal and flash-boiling evaporation conditions. An unsteady internal heat flux model and a model for the determination of the droplet surface temperature were formulated. An approximate solution to the quasi-steady energy equation was used to derive an explicit expression for the heat flux from the surrounding gas to the droplet–gas interface, with inter-diffusion of fuel vapor and the surrounding gas taken into account. The density change of the drop as a function of temperature was also considered. In order to treat phase change under trans-critical conditions, a characteristic length was defined to determine the amount of vaporized fuel as a function of time. The present vaporization models were implemented into a multi-dimensional CFD code and applied to calculate evaporation processes of single and multi-component fuel droplets and sprays for various ambient temperatures and droplet temperatures. Differences between representing model fuels using the single and multi-component fuel descriptions are discussed.

1. Introduction

The vaporization of droplets and sprays has been an issue of much interest for decades because of its significance in engineering applications. Along with experimental studies, substantial effort has been made to predict the behavior of vaporizing droplets and sprays numerically.

In internal combustion engine applications, the ranges of pressures and temperatures where fuel vaporization takes place is broad. In particular, the range of pressures and temperatures in port fuel injection (PFI) engines, gasoline direct injection (GDI) engines and homogeneous charge compression ignition (HCCI) engines with early injections is relatively low (Williams, 1973; Sirignano, 1983; Peng and Aggarwal, 1995; VanDerWege et al., 2000), whereas that in conventional compression ignition (CI) engines may be high enough that the critical state of the fuel needs to be considered (Givler and Abraham, 1996; Curtis et al., 1995; Zhu and Reitz, 2002).

For simplicity, fuels have been represented as a single component fuel in most multi-dimensional models. However, single component fuel models are not able to predict the complex behavior of the vaporization of multi-component fuels such gasoline and diesel. The preferential vaporization of light-end components in multi-component fuels affects greatly the fuel distribution near the spray and cannot be represented by single component fuel models (Lippert, 1999).

Studies have been performed on the vaporization of multi-component fuels (Tamim and Hallett, 1995; Lippert and Reitz, 1997; Zuo et al., 2000; Davy et al., 2000; Zhu and Reitz, 2002; Ra and Reitz, 2003, 2004). Multi-component fuel models are classified into two types, i.e., discrete multi-component (DMC) models and continuous multi-component (CMC) models.

The continuous multi-component model, which is based on the continuous thermodynamics method (Tamim and Hallett, 1995), represents the fuel composition as a continuous distribution function with respect to an appropriate parameter such as molecular weight. This enables a reduction of computational load while maintaining the predictability of the complex behavior of the vaporization of multi-component fuels. However, when this model is applied to combustion simulations, especially with detailed chemistry, describing the multi-component features of the fuel is inevitably limited, making it difficult to model the consumption of individual components appropriately.

On the contrary, the DMC approach tracks the individual components of the fuel during the evaporation process and allows coupling with the reaction kinetics of the individual fuel components. Although the DMC approach can have a high computational overhead due to the additional transport equations that must be solved when it is used for fuels with a large number of components, it is becoming more affordable as computational capacity has improved substantially.

Most vaporization models have focused on normal evaporation where the mass fraction of fuel vapor at the surface is less than unity, and the concept of Spalding's mass transfer number is valid (Sirignano, 1983). However, the boiling situation takes place

* Corresponding author. Tel.: +1 608 265 6759; fax: +1 608 262 6707.
E-mail address: yra@wisc.edu (Y. Ra).

0301-9322/$ - see front matter © 2008 Elsevier Ltd. All rights reserved.
doi:10.1016/j.ijmultiphaseflow.2008.10.006

frequently under practical engine operating conditions (VanDerWege, 1999; Williams et al., 2001; Schmitz et al., 2002). When fuel is injected at a higher temperature than the saturation temperature corresponding to the ambient pressure, the fuel is under superheated conditions and vaporization occurs first though the boiling process, and then changes to normal evaporation later in the droplet lifetime. For the vaporization of multi-component fuels, the droplets are more frequently in the boiling situation due to the high volatility of the light-end components of the fuel. For realistic predictions of the vaporization of multi-component fuels under typical engine operating conditions, both boiling and normal evaporation modes must be considered and the prediction of a smooth transition between those two modes is desirable.

The droplet evaporation rate predicted by conventional models is calculated by assuming that the surface temperature is equal to the droplet average temperature (Amsden, 1999). This can lead to over-prediction or under-prediction of the evaporation mass flux, depending on the ambient temperature conditions. Ra and Reitz developed a robust evaporation model that is applicable to both normal and boiling vaporization modes using a single component representation or a continuous composition distribution of the fuel (Ra and Reitz, 2003, 2004). The model was applied to simulate evaporation under various drop interior, surface and surrounding gas temperature scenarios. This included the case where the average temperature of the droplet exceeds the boiling temperature, but the surface temperature of the droplet is below the boiling temperature (e.g., when the ambient gas temperature is lower than the boiling temperature (Carey, 1992)). In the model, the physical mechanism of droplet heating/cooling was treated as heat transfer from the surface/interior to the interior/surface of the droplet that is at different temperatures. The model was applied to study boiling vaporization of multi-component fuels in engine operation.

In this paper, a DMC evaporation model, which was extended from the CMC model, is presented. An explicit form of the equation that determines the heat flux from the surrounding gas mixture to the droplet–gas interface was obtained from an approximate solution of the quasi-steady energy equation. The model was formulated to track each component of the fuel regardless of the direction of component motion, i.e., whether evaporation from the drop surface or condensation into the droplet. The model is applied to predict the vaporization of single droplets and sprays of multi-component fuels under various temperature and pressure conditions. Single component fuel cases using the model are also presented for comparison with the multi-component fuel cases.

2. Theoretical formulation

A spherical liquid droplet with a finite number of components vaporizing without chemical reactions in a gaseous environment is considered. Radiation and second order effects such as the Soret and Dufour effects are assumed to be negligible.

With the fuel components treated as discrete species and assuming no absorption of the ambient gas into the liquid droplet, the system is a discrete system consisting of the liquid phase fuel species and a discrete mixture system of vapor phase fuel and ambient gas. The general distribution function for the composition of the discrete systems is defined as

$$G_p(I) = \sum_{F=1}^{N_F} x_F^p \delta(I - I_F) + \sum_{s=1}^{N_s} x_s^p \delta(I - I_s) \tag{1}$$

where p represents v or l, denoting the properties of the vapor or liquid phases, respectively. x is the mole fraction, N the total number of discrete species, and δ is the Dirac delta function. Subscripts s and F, respectively, denote the properties of the discrete species in ambient gas and fuel liquid. The distribution has the property that

$$\sum G_p(I) = 1, \quad \sum_{s=1}^{N} x_s^p = 1 - \sum_{F=1}^{N} x_F^p \tag{2}$$

For the discrete system of the liquid fuel only, x_s^p is zero and $\sum_{F=1}^{N} x_F^p$ is unity so that $G_p(I)$ becomes equal to x_I^p, which is the mole fraction of species i in the fuel.

2.1. Liquid phase balance equation

The liquid phase is approximated as being well mixed, since mass transfer rates of the fuel components in the liquid droplets are large (Abdel-Qadera and Hallett, 2005). However, heat transfer rates are finite so the temperature in the droplet is not assumed to be uniform and a surface temperature model is introduced, as discussed later.

With no absorption of ambient gas into the spherical liquid droplet, a general form of the governing equation for the change in the liquid fuel distribution is

$$\frac{d}{dt}\left(y_{i,l}\rho_l \frac{4}{3}\pi R^3\right) = \dot{m}_i 4\pi R^2 \tag{3}$$

where ρ_l is the mass density of the liquid fuel, R is the droplet radius, and $\dot{m}_i$ is the vaporization rate of species i. The finite difference form of Eq. (3) during a given time step Δt is obtained as

$$y_{i,l,2}\rho_{l,2}\frac{4}{3}\pi R_2^3 = y_{i,l,1}\rho_{l,1}\frac{4}{3}\pi R_1^3 - \dot{m}_i 4\pi R_1^2 \Delta t \tag{4}$$

where the subscripts 1 and 2 denote the beginning and ending states of the drop, respectively.

The change of liquid drop energy is obtained from the conservation equation of energy for the two phase system consisting of the drop and the surrounding gas mixture as

$$\frac{d}{dt}\left(\int_0^R c_{v,l}\rho_l 4\pi r^2 T(r)\,dr\right) = \frac{d}{dt}\left(c_{v,l}\rho_l \frac{4}{3}\pi R^3 T_d\right) = 4\pi R^2\left(q_i - \dot{m}c_{v,l}T_s\right) \tag{5}$$

where $c_{v,l}$ is the specific heat of the liquid fuel, q_i is the heat transfer rate from the drop surface to the interior per unit area, and T_d and T_s are the average drop temperature and surface temperature, respectively. The finite difference form of Eq. (5) during a given time step Δt is

$$c_{v,l,2}\rho_{l,2}\frac{4}{3}\pi R_2^3 T_{d,2} = c_{v,l,1}\rho_{l,1}\frac{4}{3}\pi R_1^3 T_{d,1} + 4\pi R^2\left(q_i^* - \dot{m}c_{v,l}T_s^*\right)\Delta t \tag{6}$$

where q_i^* and T_s^* mean values of the heat transfer rate and the drop surface temperature, respectively, during the time step Δt.

2.2. Governing equations for gas phase

The conservation equation of species in the gas phase is

$$\frac{\partial}{\partial t}[\rho y_i] + \nabla\cdot[\rho y_i v] = \nabla\cdot(\rho D_i \nabla y_i) + s_{g,i} \tag{7}$$

where v and ρ are the velocity and density of the gas mixture, respectively, y_i and D_i are the mass fraction and diffusion coefficient of species i, and $s_{g,i}$ is the source term.

Summation of Eq. (7) over all fuel species and identification of terms in a finite difference approximation gives the species conservation equation for the two species system (fuel and air) as

$$\frac{\partial}{\partial t}[\rho y_F] + \nabla\cdot[\rho y_F v] = \nabla\cdot\left(\rho\overline{D}\nabla y_F\right) + S_g \tag{8}$$

where y_F is the total mass fraction of fuel species, $\overline{D}$ is the average diffusion coefficient of the fuel species, and S_g is the total source term.

The energy conservation equation for the gas phase is

$$\overline{C}_P \frac{\partial}{\partial t}(\rho T) + \overline{C}_P \nabla \cdot (\rho v T) = \nabla \cdot \lambda \nabla T + \left(\overline{C_{PF} D_F} - C_{PA}\overline{D}\right)\rho \nabla y_F \cdot \nabla T \tag{9}$$

where T is the temperature, λ is the thermal conductivity, $\overline{C}_P$ is the mixture specific heat, C_{PA} is the specific heat of air, and $\overline{C_{PF}D_F}$ is the average value of the product of specific heat and the diffusion coefficient of the fuel species. The last term in Eq. (9) represents energy transport due to inter-diffusion of species.

2.3. Vapor–liquid equilibrium

The equilibrium at the interface between the liquid droplet and the surrounding gas is based on the assumption that the chemical potential μ for the liquid phase, l, and the vapor phase, v, are equal for each species, i. Assuming an ideal solution, the surface mass fraction of fuel vapor can be determined using Raoult's law. For a mixture of discrete components, Raoult's law is

$$p_{i,v} = x_{i,v} P = x_{i,l} P_{sat,i} \tag{10}$$

where p_i is the partial pressure of species i in the vapor phase at the droplet surface, $P_{sat,i}(T)$ is the vapor pressure of species i at temperature T, x is the mole fraction and the subscripts v and l denote the vapor phase and liquid phases, respectively. The species vapor pressure is given by the Clausius–Clapeyron equation.

The quantities $x_{i,l}$ and $y_{i,v}$ are determined from the relationship between mole and mass fractions:

$$x_{i,l} = \frac{y_{i,l}/W_i}{\sum_{j=1}^{N}(y_{j,l}/W_j)}, \quad y_{i,v} = \frac{x_{i,v}W_i}{\sum_{j=1}^{N}(x_{j,v}W_j)} = \frac{p_{i,v}W_i}{\sum_{j=1}^{N}(p_{j,v}W_j)} \tag{11}$$

where y is mass fraction, and W_i is the molecular weight of species i.

2.4. Determination of surface temperature

The surface temperature of the droplet is determined from a heat and mass transfer balance at the interface between the droplet and the surrounding gas. There are two regimes of heat transfer, i.e., heat transfer occurring from the inside of the droplet to the surface, q_i, and heat transfer occurring from the outer gas to the surface, q_o. The rate of heat transfer balances the required heat for vaporization at the surface

$$L(T_s)\dot{m} = q_i + q_o \tag{12}$$

where $L(T_s)$ is the latent heat of the fuel at the surface temperature, T_s, and $\dot{m}$ is the mass vaporization rate. The heat transfer from inside the droplet was modeled as a convective heat transfer process with internal circulation taken into account. The heat transfer coefficient inside the droplet is determined from the thermal conductivity, λ, and the unsteady equivalent thickness of the thermal boundary layer, δ_e, as

$$q_i = h_{i,eff}(T_d - T_s) = \frac{\lambda}{\delta_e}(T_d - T_s) \tag{13}$$

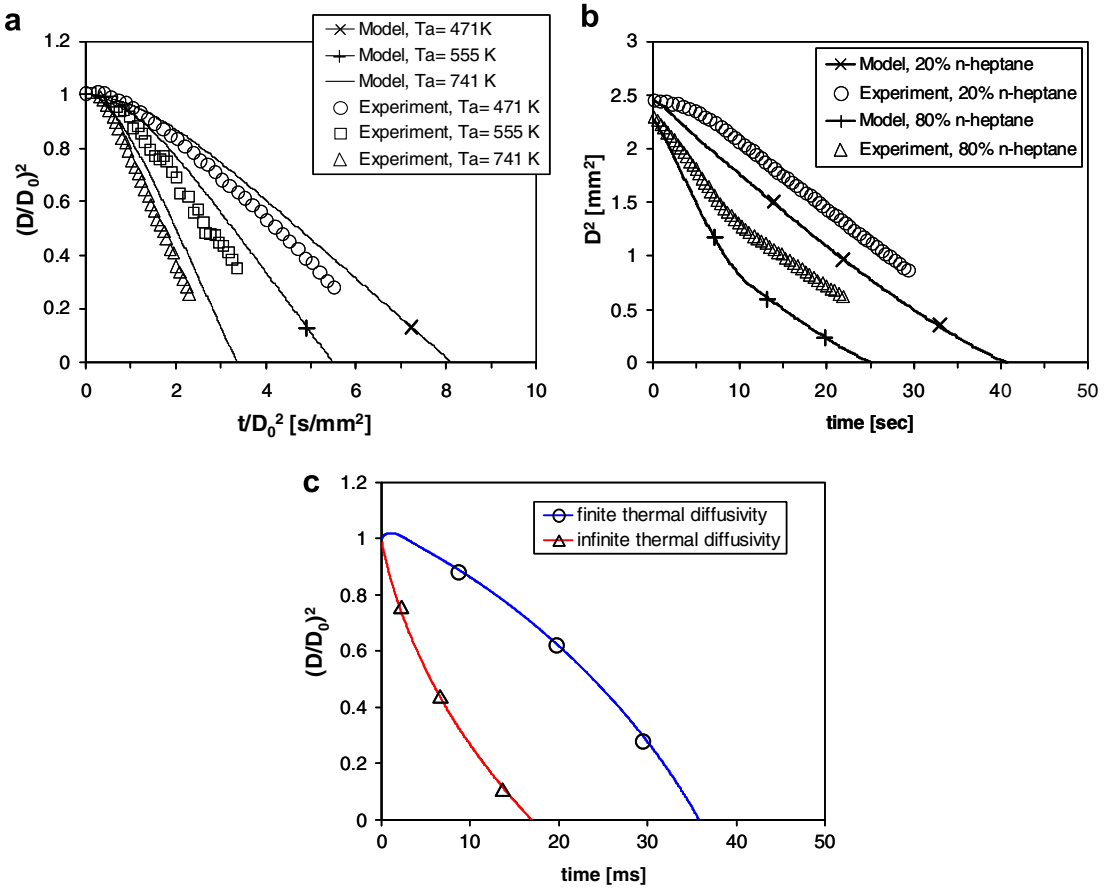

Fig. 1. Experimental comparisons and effect of thermal diffusivity model. (a) Stationary n-heptane droplet evaporation comparison with experiments of Nomura et al. (1996) for ambient pressure of 1 bar, initial drop diameter of 0.6 mm, (b) convective binary (n-heptane and n-decane) component droplet evaporation comparison with experiments of Gökalp et al. (1994) for ambient pressure, 1 bar, ambient temperature, 372 K, and flow velocity, 1.45 m/s, (c) comparison of predicted single tetra-decane ($C_{14}H_{30}$) drop evaporations using finite and infinite thermal diffusion rates for ambient pressure, 10 bar, ambient temperature, 800 K, initial drop diameter, 100 μm, and initial droplet velocity, 50 m/s.

where T_d is the droplet interior temperature, T_s is the droplet surface temperature, and δ_e is calculated using an effective thermal diffusivity (Sirignano, 1983)

$$\delta_e = \sqrt{\pi \alpha_{eff} t} = \sqrt{\pi \chi \alpha_l t} \tag{14}$$

where $\chi = 1.86 + 0.86\tanh[2.225\log_{10}(Pe_l/30)]$ and Pe_l is the Peclet number of the droplet.

The effective heat transfer coefficient for the outer flux is determined from an approximate solution of the energy equation for the vapor phase with the effects of inter-diffusion and Stefan flow considered (see Appendix A in Electronic Annex 1). Solving the energy equation, Eq. (9) near the droplet surface gives the heat flux equation as

$$q_o = \frac{\kappa \overline{C}_P \dot{m}}{\exp\left[\frac{2r_o \overline{C}_P \dot{m}}{\lambda Nu} - \frac{[C_A](y_{Fsur} - y_{Fo})}{\lambda}\frac{Sh}{Nu}\right] - 1}(T_{sur} - T_s) = h_{o,eff}(T_{sur} - T_s) \tag{15}$$

where r_o is the droplet radius, Sh is the Sherwood number, Nu is the Nusselt number, $\overline{C}_P$ is the average specific heat of the gas mixture including fuel vapor, κ is a correlation factor defined by Ra and Reitz (2003), $[C_A]$ is the inter-diffusional difference of energy flux between fuel and air, $\rho\left(\overline{C_{PF}D_F} - C_{PA}\overline{D}_F\right)$, $\overline{D}_F$ is the average diffusion coefficient of fuel species, y_{Fo} and y_{Fsur} are the mass fractions of fuel at the interface and far away, respectively, and T_{sur} is the surrounding gas temperature.

Inserting Eqs. (13) and (15) into Eq. (12) gives an explicit equation that relates the vaporization rate, $\dot{m}$, to the temperatures of the droplet and the surrounding gas mixture as

$$\dot{m}L(T_s) = h_{i,eff}(T_d - T_s) + \frac{\kappa \overline{C}_P \dot{m}}{\exp\left[\frac{2r_o \overline{C}_P \dot{m}}{\lambda Nu} - \frac{[C_A](y_{Fsur} - y_{Fo})}{\lambda}\frac{Sh}{Nu}\right] - 1}(T_{sur} - T_s) \tag{16}$$

The rate of mass transport at the droplet surface is calculated using the well-known high mass transfer rate equation with Spalding's transfer number (Sirignano, 1983)

$$\dot{m} = g_m \ln(1 + B_M) \tag{17}$$

where g_m is the mass transfer coefficient determined from $g_m = Sh\rho\overline{D}/2R$, and B_M is Spalding's transfer number, $(y_{Fs} - y_{Fsur})/(1 - y_{Fs})$.

Since the effective heat transfer coefficient for the outer heat flux is coupled with the vaporization rate, the surface temperature of the droplet is determined by solving two balance equations iteratively, and assuming a quasi-steady heat transfer process.

2.5. Modeling the boiling process

Assuming that (1) the droplet surface distortion can be neglected so that the droplet maintains its spherical shape, (2) there is no sudden break-up of the droplet due to internal phenomena such as micro-explosions, and (3) the droplet surface temperature remains at the boiling temperature as long as the assumption of equilibrium is valid, the formulation of Eq. (15) is applied for the boiling case by setting the surface temperature equal to the boiling temperature, T_b, and surface mass fraction to unity. Note that the vaporization rate calculated based on Spalding's mass transfer number (Eq. (17)) is no longer valid because it diverges to an infinite value. A similar formulation to Eq. (16) can be obtained as

$$\dot{m}L(T_b) = (h_{i,eff,s} + \alpha_{sh})(T_d - T_b) + \frac{\kappa \overline{C}_P \dot{m}}{\exp\left[\frac{2r_o \overline{C}_P \dot{m}}{\lambda Nu} - \frac{[C_A](y_{Fsur} - 1)}{\lambda}\frac{Sh}{Nu}\right] - 1}(T_{sur} - T_b) \tag{18}$$

where $h_{i,eff,s}$ is the coefficient for the contribution of heat transfer by internal circulation at the saturation temperature, α_{sh} is the heat transfer enhancement through the effect of nucleation which is modeled using the correlation of Adachi et al. (1997). Detailed description of the boiling process modeling is given in Appendix B in Electronic Annex 1.

The vaporization rate determined from the energy and mass transfer equations (for normal evaporation cases) is used to calculate the source terms for the vapor phase transport equations, Eq. (8).

2.6. Calculation of average properties of liquid and vapor phase fuel

Assuming the liquid fuel to be an ideal mixture of multi-components, average thermal and transport properties of the liquid phase

Table 1
Numerical conditions for single drop evaporation simulations.

Fuel: gasoline, iso-octane	
Initial drop diameter (μm)	100
Initial fuel temperature (K)	313–390
Ambient pressure (bar)	0.3–2
Ambient temperature (K)	500–800
Components	iC_5H_{12}, iC_6H_{14}, iC_7H_{16}, iC_8H_{18}, C_9H_{20}, $C_{10}H_{22}$, and $C_{12}H_{26}$
Fuel: diesel, tetra-decane	
Initial drop diameter (μm)	100
Initial fuel temperature (K)	330–390
Ambient pressure (bar)	0.4–40
Ambient temperature (K)	500–1000
Components	C_7H_8, $C_{10}H_{22}$, $C_{12}H_{26}$, $C_{14}H_{30}$, $C_{16}H_{32}$, and $C_{18}H_{34}$

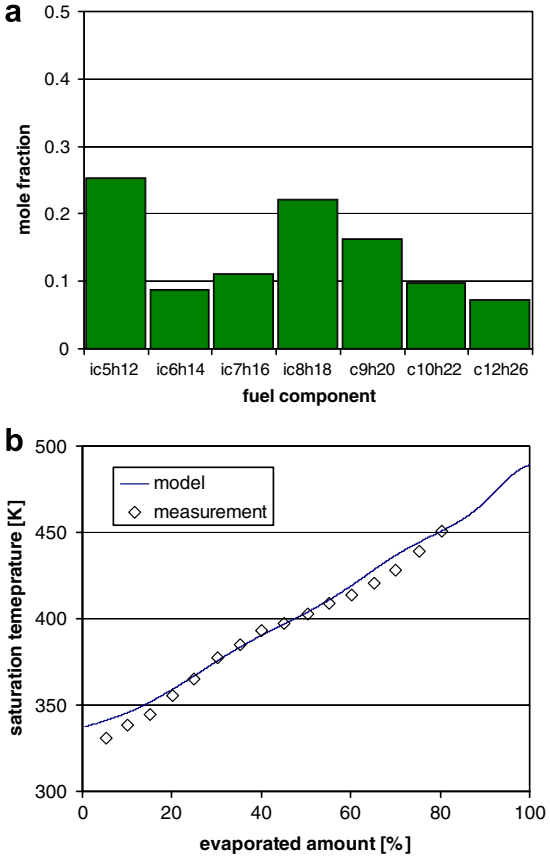

Fig. 2. Modeled composition and distillation curve of gasoline fuel. Measurement data are from Smith and Bruno (2007). (a) Mole fraction of components and (b) comparison of distillation curves between modeled and measured data.

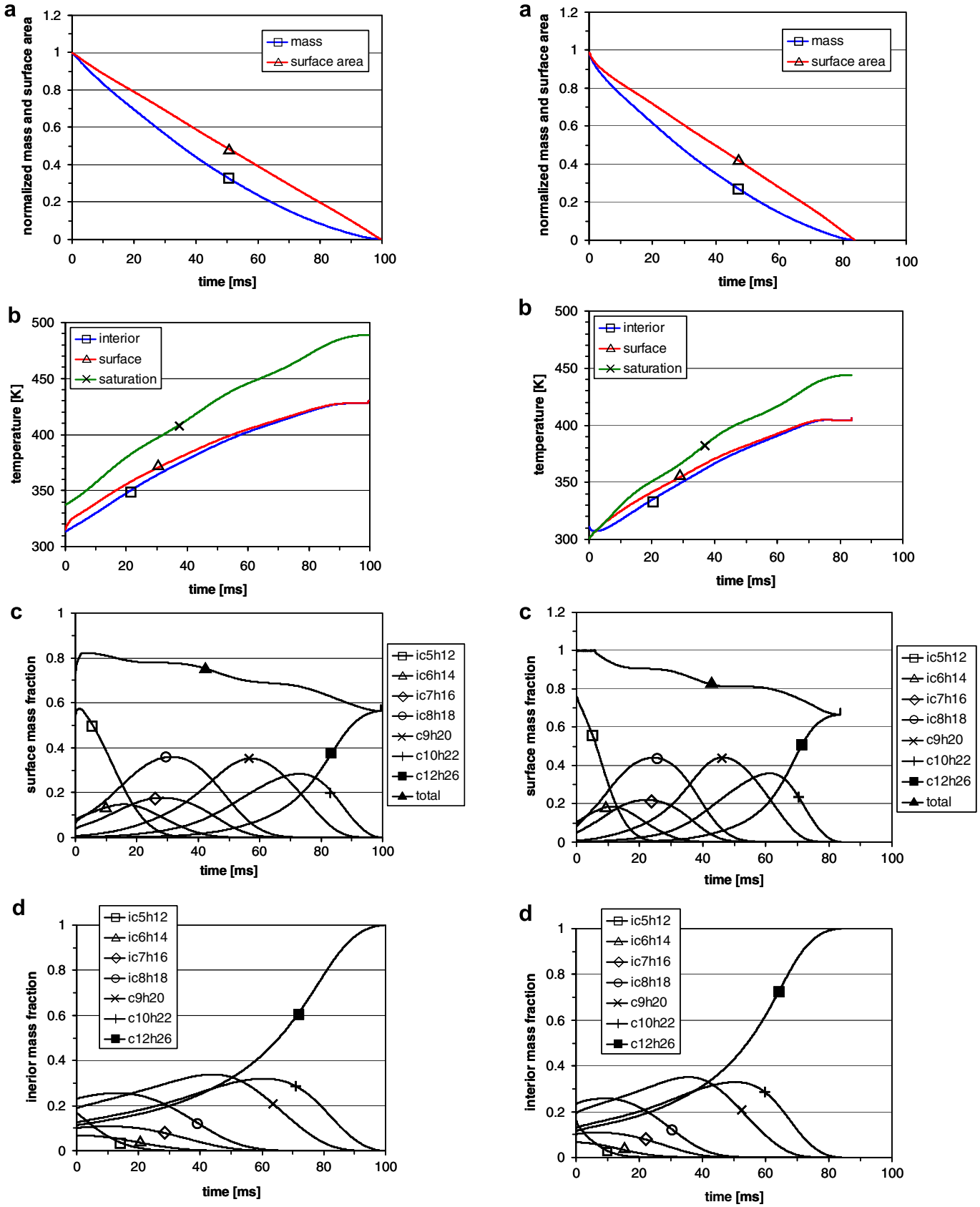

Fig. 3. Normal evaporation of a single gasoline drop. $D_o = 100$ μm and $T_{d,o} = 313$ K, $P_o = 1$ bar, $T_o = 500$ K. (a) Normalized drop mass and surface area, (b) drop interior, surface and saturation temperature, (c) surface mass fraction of fuel components, and (d) drop interior fuel component mass fractions.

Fig. 4. Evaporation of a single superheated gasoline drop. $D_o = 100$ μm and $T_{d,o} = 313$ K, $P_o = 0.3$ bar, $T_o = 500$ K. (a) Normalized drop mass and surface area, (b) drop interior, surface and saturation temperature, (c) surface mass fraction of fuel components, and (d) drop interior fuel component mass fractions.

can be defined (Fuller et al., 1969; Strehlow, 1985; Daubert and Danner, 1999; Stradi et al., 2001). Also, the properties fuel vapor–air mixtures are calculated based on the gas phase properties of the individual fuel components. The fuel properties considered in the present study include the density of the liquid fuel, vapor pressure, surface tension, liquid viscosity and thermal conductivity, heat of vaporization, liquid heat capacity, fuel vapor diffusivity, thermal conductivity and viscosity. Detailed information about the correlations and formulations of the properties are described in Appendix C in Electronic Annex 1.

3. Spray sub-models

For simulating the spray and the mixing of fuel/air mixtures in a constant volume chamber, various physical sub-models were employed in the CFD code. The sub models include models related to drop breakup (Beale and Reitz, 1999), collision and coalescence (Amsden, 1999), drop deformation (Liu et al., 1993), etc. Detailed information of the sub-models employed in the present study is given in Appendix E in Electronic Annex 1.

4. Results and discussion

The present DMC fuel vaporization model has been implemented in the multi-dimensional CFD code, KIVA3V Release-2 (Amsden, 1999) and was applied to study the vaporization of single stagnant droplets and sprays. For single drop evaporation simulations, various fuel temperatures, ambient gas pressures and temperatures were considered in order to assess the performance of the model in both the normal and flash-boiling vaporization modes. Evaporation of typical gasoline and diesel fuels were modeled and compared with the results for their single component surrogate fuel counterparts, i.e., iso-octane and tetra-decane, respectively. Also, the present model was applied to simulate the vaporization of single and multi-component fuel sprays injected into a constant volume chamber.

4.1. Single drop evaporation

4.1.1. Experimental comparison

The model is compared with experimental results of Gökalp et al. (1994) and Nomura et al. (1996) for single and binary component droplet evaporation. Fig. 1(a) shows comparisons of drop size change history of *n*-heptane droplets under stationary, micro-gravity conditions. The present model predictions are in good agreement with the experimental measurements (Nomura et al., 1996) for various ambient temperatures. In Fig. 1(b), the evaporation of binary component fuel droplets suspended in a convective condition is compared with experimental results of Gökalp et al. (1994). Although the simulation results slightly overpredict the evaporation in early stage in both fuel composition cases, the evaporation constants in the later stage of evaporation are well predicted and the change of evaporation constants (negative of the rate of change of drop surface area) as the fuel composition changes due to preferential vaporization of the fuel components are clearly captured, especially for the higher *n*-heptane composition case. Note that the present model assumes uniform distribution of fuel components within a droplet. Thus, the vaporization of light end components, which preferably vaporize at the surface of the droplet, tends to be slightly overestimated. This explains, in part, why the simulation results show faster evaporation than experiments at the early stage of vaporization. Another reason for the discrepancy may be the effect of heat transfer from the droplet to the drop-holding fiber, which was not considered in the computations. Fig. 1(c) shows the comparison of simulation results using finite and infinite thermal diffusion rates for a tetra-decane droplet injected at

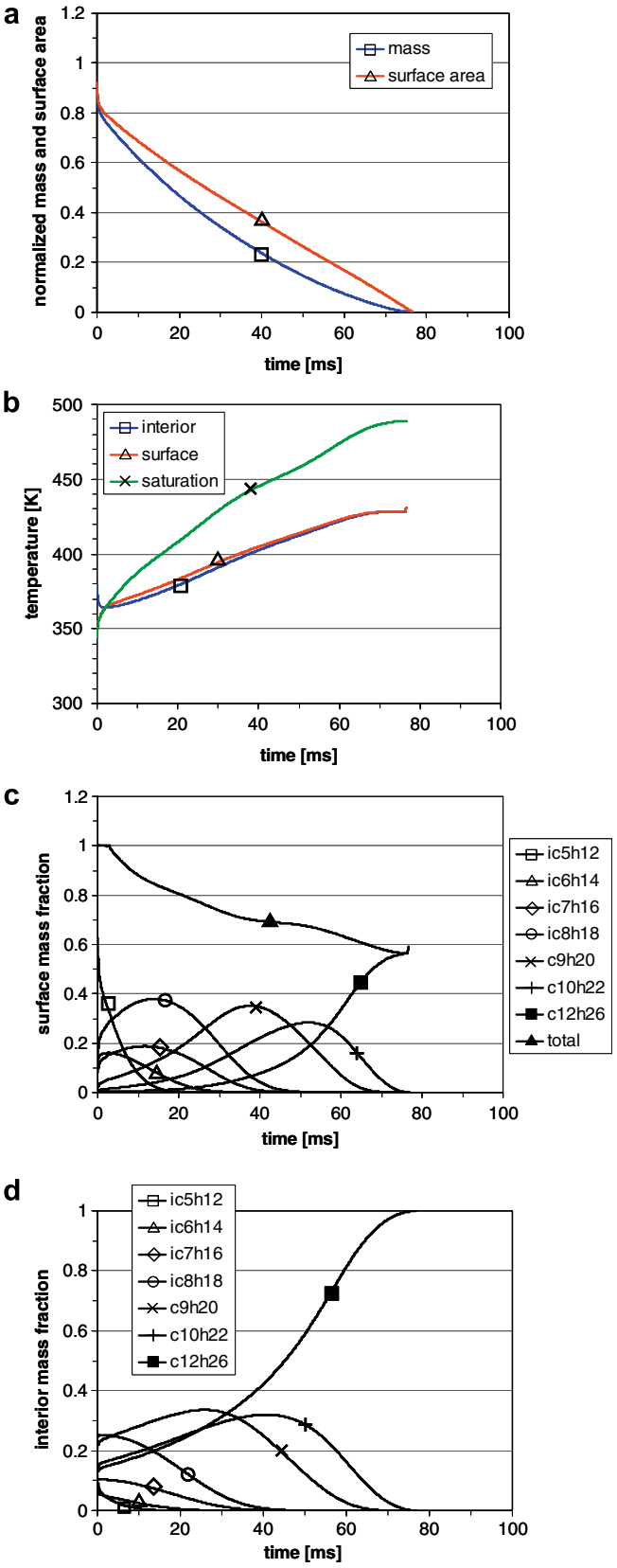

Fig. 5. Evaporation of a single superheated gasoline drop. $D_o = 100\ \mu m$ and $T_{d,o} = 390$ K, $P_o = 1$ bar, $T_o = 500$ K. (a) Normalized drop mass and surface area, (b) drop interior, surface and saturation temperature, (c) surface mass fraction of fuel components, and (d) drop interior fuel component mass fractions.

50 m/s into quiescent air. The initial drop diameter was 100 μm. The drop lifetime and evaporation constants were significantly affected by the thermal diffusion rate. The swelling of the droplet could not be captured using the infinite thermal diffusion rate model since the droplet heating was significantly underpredicted.

4.1.2. Multi-component drop evaporation

4.1.2.1. Gasoline drop evaporation. Evaporation of a single gasoline drop was simulated using the present model. In order to model the composition of typical gasoline fuel, seven hydrocarbon species were considered, as listed in Table 1. The composition and distillation curve of the modeled fuel are shown in Fig. 2. The average molecular weight of the modeled fuel is 108.5 g/mol. The predicted distillation characteristics of the fuel are in good agreement with the measured data of Smith and Bruno (2007). Although the components employed in the model may not represent all of the actual chemical components found in practical pump gasoline fuels, the selected paraffin fuels were considered adequate to demonstrate the performance of the present multi-component evaporation model.

Various conditions were tested to validate the evaporation model. Drop temperatures were varied between 313 and 390 K to simulate the flash boiling regime, as well as the normal evaporation regime at atmospheric pressure. Also, variation of the ambient pressure between 0.3 and 2 bar was considered. Lowering the ambient pressure tends to lead to a superheated drop condition. Ambient temperatures between 500 and 800 K were tested. The initial drop size was fixed at 100 μm for the single drop simula-

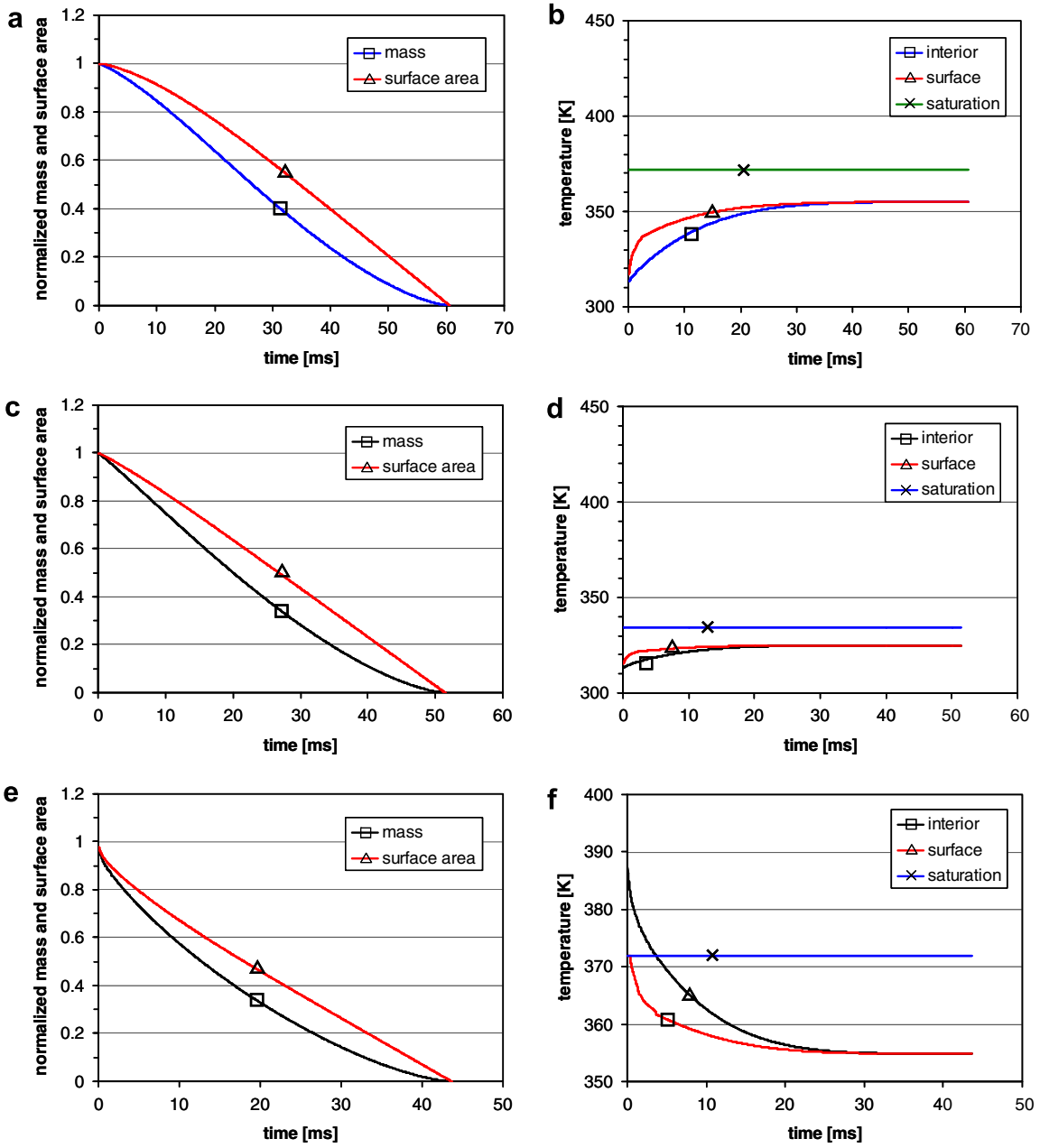

Fig. 6. Evaporation of a single iso-octane drop. D_o = 100 μm and T_o = 500 K. (a) Normalized drop mass and surface area for $T_{d,o}$ = 313 K, P_o = 1 bar, (b) drop interior, surface and saturation temperatures for $T_{d,o}$ = 313 K, P_o = 1 bar, (c) normalized drop mass and surface area for $T_{d,o}$ = 313 K, P_o = 0.3 bar, (d) drop interior, surface and saturation temperature for $T_{d,o}$ = 313 K, P_o = 0.3 bar, (e) normalized drop mass and surface area for $T_{d,o}$ = 390 K, P_o = 1 bar, and (f) drop interior, surface and saturation temperature for $T_{d,o}$ = 313 K, P_o = 1 bar.

tions. The detailed numerical conditions for the gasoline drop evaporation study are listed in Table 1.

Fig. 3 shows the behavior under normal evaporation conditions of a multi-component gasoline droplet in terms of its variation of drop mass, drop surface area, the temperatures of the drop's interior and surface, the saturation temperature, and the component mass fractions in the drop interior and at the surface. The initial drop temperature was 313 K, and the ambient pressure and temperature were 1 bar and 500 K, respectively.

The drop size varies in the manner of well-known D^2-law, as shown in Fig. 3(a). The average evaporation constant for the case was 0.1004 mm^2/s. Fig. 3(b) shows an interesting characteristic of multi-component fuel vaporization; due to preferential vaporization of the more volatile light-end components, the composition of the droplet changes continuously, and thus gasoline droplets do not reach an equilibrium condition, as in the corresponding case of the single component iso-octane droplet (shown later in Fig. 6).

From the beginning the droplet is heated by the heat flux from the hot ambient gas. Note, however, that the droplet surface temperature adjusts in order for the energy and mass balance to be satisfied, and the droplet experiences heating and/or cooling processes, depending on the temperature configuration surrounding the vaporizing droplet. The difference between the drop surface and interior temperatures decreases as the drop size decreases with time, as expected.

During the drop life time the total mass fraction of fuel components at the drop surface is less than unity, which confirms that vaporization occurs in the normal evaporation regime, as shown in Fig. 3(c). As is expected the surface mass fraction of the light-end component (iC_5H_{12}) is high during the early period of evaporation and then it rapidly decreases as the vaporization proceeds. At the last stage of evaporation only the heavy-end component ($C_{12}H_{26}$) remains in the droplet, as can be seen from the drop interior fuel components shown in Fig. 3(d).

When the ambient gas pressure is reduced such that the saturation pressure is higher than the ambient pressure, the droplet condition becomes superheated. The evaporation behavior of a superheated droplet is shown in Fig. 4. The ambient pressure was 0.3 bar, while the other conditions are the same as in Fig. 3. For the ambient pressure of 0.3 bar, the initial saturation temperature is 300.66 K. Therefore, the drop surface temperature is expected to become the corresponding saturation temperature and the surface fuel mass fraction to become unity. In this case, the droplet vaporizes in the flash-boiling mode, which can be seen from the rapid decrease of drop surface area shown in Fig. 4(a). This flash-boiling evaporation is also confirmed from the results of the drop surface temperature and fuel mass fraction profiles before 5.9 ms, as shown in Fig. 4(b) and (c), respectively. Compared to the normal evaporation case shown in Fig. 3, boiling evaporation results in a much shorter drop life time. Since the drop surface temperature is lower than the drop interior temperature initially, the droplet actually experiences a cooling process. This aids the evaporation of fuel at the drop surface because the internal energy of the droplet also supplies part of the latent heat required to vaporize the fuel. However, it is notable that the droplet surface temperature adjusts in order for the energy and mass balance to be satisfied and the droplet may experience heating and/or cooling processes, depending on the temperature configuration around the vaporizing droplet. After a certain time (~2.1 ms in this case), the drop temperature becomes lower than the surface temperature and the droplet is heated, which can be seen in Fig. 4(b). Note that, since mass transfer within the drop inside is assumed to be negligible in the present model, the relative shapes of the profiles of the surface and interior mass fractions of the components are similar between the normal and boiling evaporation cases, while the drop life times are different.

Flash-boiling can also be promoted when fuel is heated within an injector nozzle before injection. An initial drop temperature of 390 K was used to investigate this case. The other conditions were the same as in Fig. 3. The saturation temperature is calculated to be 337.35 K for an ambient pressure of 1 bar with the initial composition of the present gasoline model fuel. As shown in Fig. 5(a), within a short period of time (~3 ms), the drop surface area is rapidly reduced to 80% of its initial value due to flash-boiling (the initial evaporation constant was as high as 14.1 mm^2/s). Subsequently, the evaporation mode changes quickly to the normal evaporation mode. In the increased initial drop temperature case the drop interior temperatures reach higher values (~428 K) than those in the reduced ambient pressure case (~404 K) (see Fig. 4), since the surface fuel mass fraction is reduced to lower values.

The behavior of iso-octane single droplet vaporization is shown in Fig. 6 for conditions corresponding to the gasoline droplet cases shown in Figs. 3 and 4. Since the vapor pressure of iso-octane is much lower than the light-end component of the present gasoline model (iC_5H_{12}), the evaporation rate becomes lower than that of the corresponding gasoline case. Therefore, more heat from the surrounding gases is used to heat up the droplet, and thus the drop interior and surface temperatures, and their difference increase faster than in the gasoline case.

Due to the reduction of the liquid density with increasing temperature drop heating has a noticeable swelling effect on the drop size, with the result that the drop size decreases much slower ini-

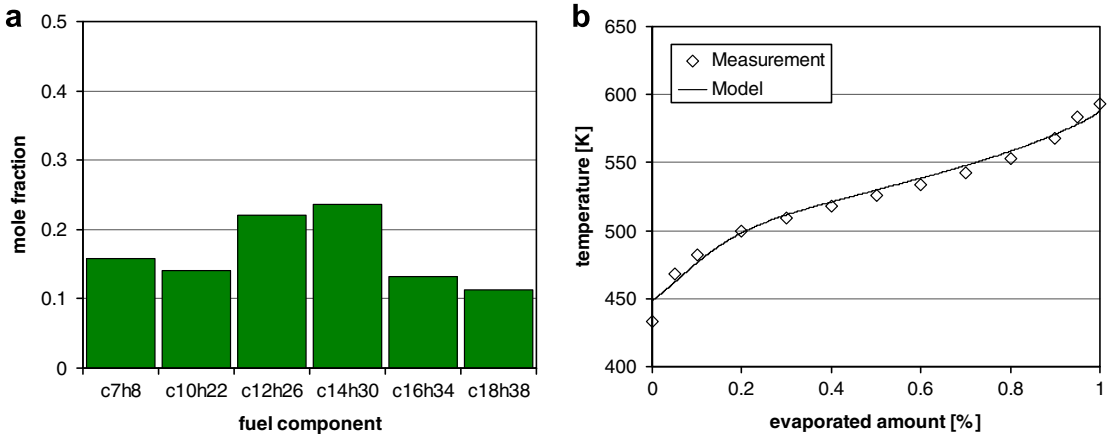

Fig. 7. Modeled composition and distillation curve of a typical diesel fuel. Measured data are from Butts (2008). (a) Mole fraction of components and (b) comparison of distillation curves between modeled and measured data.

tially than in the corresponding gasoline case, as shown in Fig. 6(a). The initial evaporation constant was reduced to 0.008 mm^2/s. However, at the later stages of evaporation, the evaporation rate of the iso-octane droplet become higher than that of the gasoline droplet, because the remaining fuel components in the gasoline droplet become heavier than iso-octane. This results in higher evaporation constants (~0.194 mm^2/s) in the iso-octane droplet case, and the eventual drop life time becomes shorter than that of the gasoline droplet case. As mentioned above, the evaporation of a single component droplet also reaches an equilibrium condition at which all the heat fluxes from the surrounding gas is used to supply the latent heat for evaporation and the drop temperature is maintained constant, as shown in Fig. 6(b).

By reducing the ambient pressure, the evaporation of iso-octane droplets is enhanced. Fig. 6(c) and (d) shows the profiles of drop mass, drop surface area, drop interior and surface temperatures, and the saturation temperature of a vaporizing iso-octane droplet at an ambient pressure of 0.3 bar. The drop life time is shortened due to the increased fuel mass fraction at the drop surface. However, different from the corresponding gasoline case, it is predicted that flash-boiling evaporation does not occur since the saturation temperature (334 K) at 0.3 bar is higher than the initial drop temperature (313 K) and the equilibrium temperature (325 K) is lower than the corresponding saturation temperature.

However, when the initial drop temperature is increased to 390 K, iso-octane droplets start vaporizing in the flash-boiling mode. Thereafter, the mode changes to normal evaporation after a short time (~0.46 ms). It is interesting that the drop interior is still in the superheated condition until ~3.7 ms, while the surface temperature becomes lower than the saturation temperature at 1.0 bar. Therefore, the evaporation constants become pretty constant during most of the drop life time, except for during the flash boiling period. It is also notable that the iso-octane droplet is predicted to experience cooling over the entire drop life time, which is a significant difference from the multi-component gasoline drop case.

4.1.2.2 Effects of ambient pressure, ambient temperature and drop temperature in gasoline drop evaporation. The effects of the variation of ambient pressure, ambient temperature, and initial drop temperature on single gasoline drop evaporation were also investigated. Due to the limitation of paper length, detailed presentation of the results is omitted. The results are available in Electronic Annex 2.

4.1.2.3. Diesel drop evaporation. The present model was also applied to consider the evaporation of a single diesel fuel drop. In order to model the composition of a typical diesel fuel, six hydrocarbon species were considered whose molecular weights range from 92 to 254, as listed in Table 1. The composition and distillation curve of the modeled diesel fuel are shown in Fig. 7. The average molecular weight of the modeled fuel is 177.1 g/mol. The predicted distillation characteristics of the fuel are in excellent agreement with measured data of Butts (2008). Since the volatility of diesel fuel components is much lower than those of gasoline, the distillation temperatures are much higher than those of gasoline. In the diesel fuel cases, toluene (C_7H_8) was included in the composition to be able to also consider aromatic components that represent a significant portion of the fuel composition in typical diesel fuel (Owen and Coley, 1995).

Various conditions of drop initial temperature, ambient pressure and temperature were simulated. The initial drop temperature ranged from 330 to 390 K. The ambient gas pressure was changed from 0.4 to 40 bar and the ambient gas temperature was varied from 500 to 1000 K. As in the gasoline/iso-octane study, the initial drop size was 100 μm and the detailed numerical conditions for the diesel drop evaporation study are listed in Table 1.

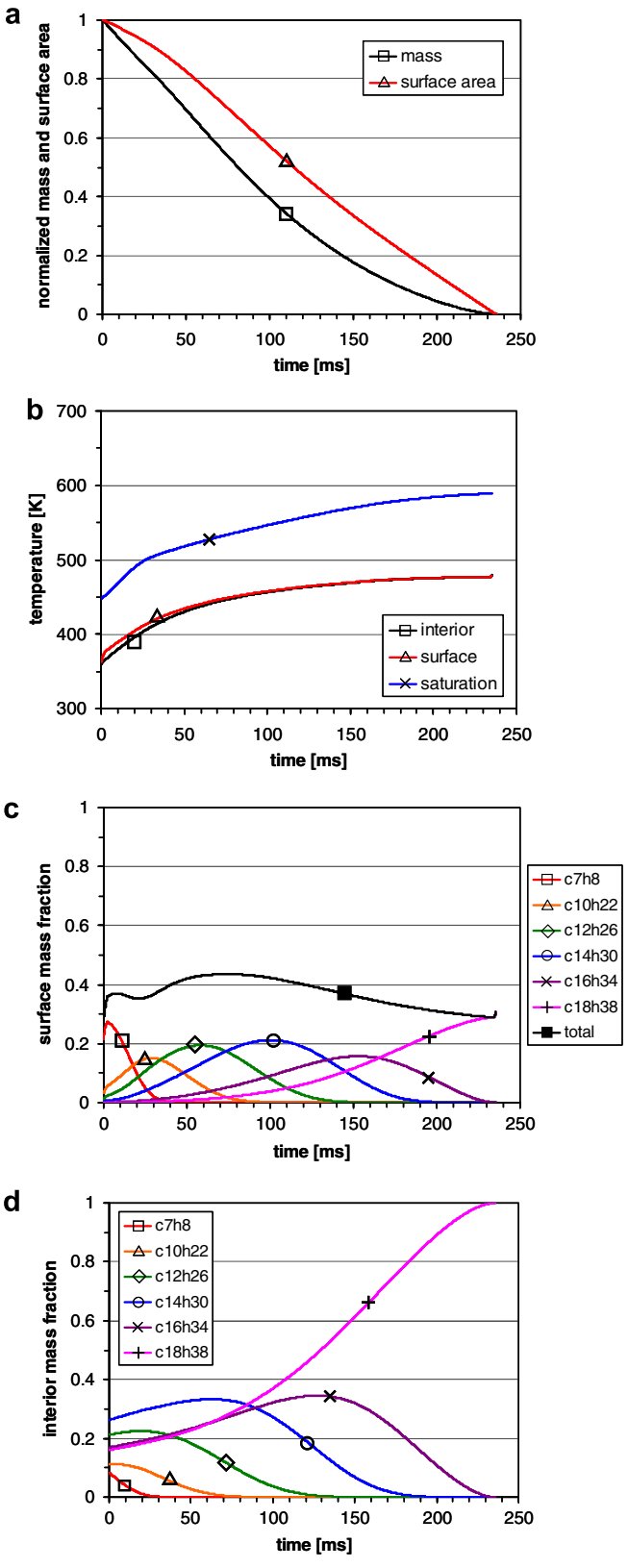

Fig. 8. Normal evaporation of a single diesel drop. D_o = 100 μm and $T_{d,o}$ = 360 K, P_o = 1 bar, T_o = 500 K. (a) Normalized drop mass and surface area, (b) drop interior, surface and saturation temperatures, (c) surface mass fraction of fuel components, and (d) drop interior fuel component mass fractions.

Fig. 8 shows the predicted behavior of diesel drop evaporation in terms of the variation of drop mass, drop surface area, the drop interior, surface and saturation temperatures, and the fuel component mass fractions at the drop interior and surface. The initial drop temperature was 360 K, and the ambient pressure and temperature were 1 bar and 500 K, respectively. The evaporation process is seen to be very similar to that of gasoline (see Fig. 3) except for the deviation of the drop surface area profile from linearity and the lower levels of total fuel mass fraction at the drop surface due to the lower volatility of the modeled diesel fuel components.

Due to the differences in fuel composition from gasoline, the total fuel mass fraction at the drop surface is predicted to increase for a longer time (~80 ms), and then to decrease gradually, as shown in Fig. 8(c). In the mean time, the evaporation constants increase up to 0.052 mm^2/s, and then decrease to 0.038 mm^2/s at the end of the drop life time. It is clearly seen from Fig. 8(d) that the lightest component vaporizes first and the heaviest component becomes dominant in the fuel composition during the final stage of evaporation.

On the contrary, the evaporation of a single tetra-decane ($C_{14}H_{30}$) droplet shows a very different drop size variation history, especially in the early stages of evaporation, as shown in Fig. 9. Since the volatility of tetra-decane is much lower than those of the three light-end components of diesel considered in the present model, the evaporation rate at the beginning of the evaporation is lower than the multi-component diesel case. Thus, more energy is transferred into the drop interior to heat up the droplet, which leads to a decrease in the fuel drop density, resulting in noticeable swelling of the droplet. This is clearly seen from the profile of the normalized surface area that exceeds unity and increases until 17 ms. Also, the evaporation constants tend to approach a constant value as the drop surface condition reaches the equilibrium state.

As in the gasoline cases, when the ambient gas temperature is elevated, the surface of diesel droplets can reach the saturated condition. Fig. 10 shows the variation of drop mass, drop surface area, the drop interior, surface and saturation temperatures, and the component mass fractions at the drop interior and surface for an ambient gas temperature of 800 K. All other conditions are the same as those in Fig. 8.

The fuel droplet is heated rapidly through heat transfer from the surrounding gases and the fuel vapor pressures are increased. After the surface fuel mass fraction becomes unity (see Fig. 10(c)), the saturation and drop surface temperatures increase simultaneously as the lighter components vaporize preferentially. Since the drop interior temperatures stay lower than the surface temperatures, the droplet continues being heated, as shown in Fig. 10(b). It is predicted that the evaporation constants change continuously over the entire evaporation period.

The fuel composition becomes heavier as the evaporation proceeds, and the droplet temperature increases, but the temperature difference between the drop interior and surface decreases. Thus, the surface condition may repeatedly change to the normal evaporation mode. This results in a slower evaporation, which is seen as a slight bump at the later stage of the evaporation (~47 ms) in the drop surface area profile in Fig. 10(a).

When the ambient gas pressure is elevated, initial drop swelling is increased due to the decreased surface fuel mass fraction and the increased heat transfer into the drop interior. Fig. 11 shows the evaporation behavior of a single diesel droplet for ambient pressure of 10 bar. The normalized drop surface area exceeds unity while the droplet is rapidly heated, as shown in Fig. 11(a). After a sufficient time (~63 ms), the surface condition reaches the boiling state. By this time, it is predicted that most of the light-end components have vaporized.

For the corresponding conditions, it was predicted that a single tetra-decane drop does not experience boiling evaporation during the entire drop life time. Fig. 12 shows the profiles of normalized drop surface area, drop interior and surface temperatures, and the saturation temperature of a tetra-decane droplet vaporizing at 10 bar. As described above, the predicted drop life time is shorter than that of the multi-component diesel droplet. Similar drop surface area variation to that of the diesel droplet is seen in Fig. 12(a). However, the drop surface temperature is predicted to be lower than the corresponding saturation temperature, as shown in Fig. 12(b).

4.1.2.4. Effects of ambient pressure, ambient temperature and drop temperature in diesel drop evaporation. The effects of the variation of ambient pressure, ambient temperature, and initial drop temperature on single diesel drop evaporation were also investigated. Due to the limitation of paper length, detailed presentation of the results is omitted. The results are available in Electronic Annex 2.

4.2. Spray vaporization

The present evaporation model was also applied to simulate the vaporization process of gasoline and diesel sprays injected into a constant volume chamber. Assuming a 7-hole injector, a 1/7th sector of a cylindrical computational grid was used for

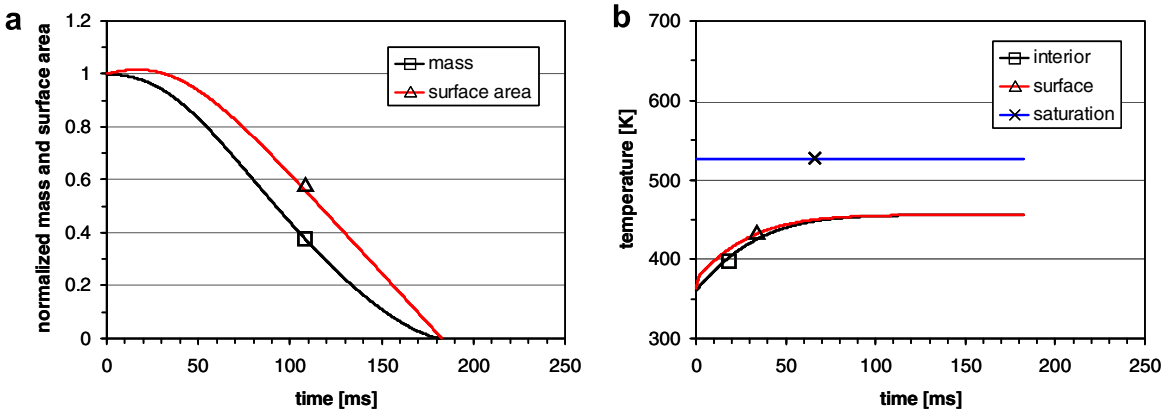

Fig. 9. Normal evaporation of a single tetra-decane drop. D_o = 100 μm and $T_{d,o}$ = 360 K, P_o = 1 bar, T_o = 500 K. (a) Normalized drop mass and surface area and (b) drop interior, surface and saturation temperatures.

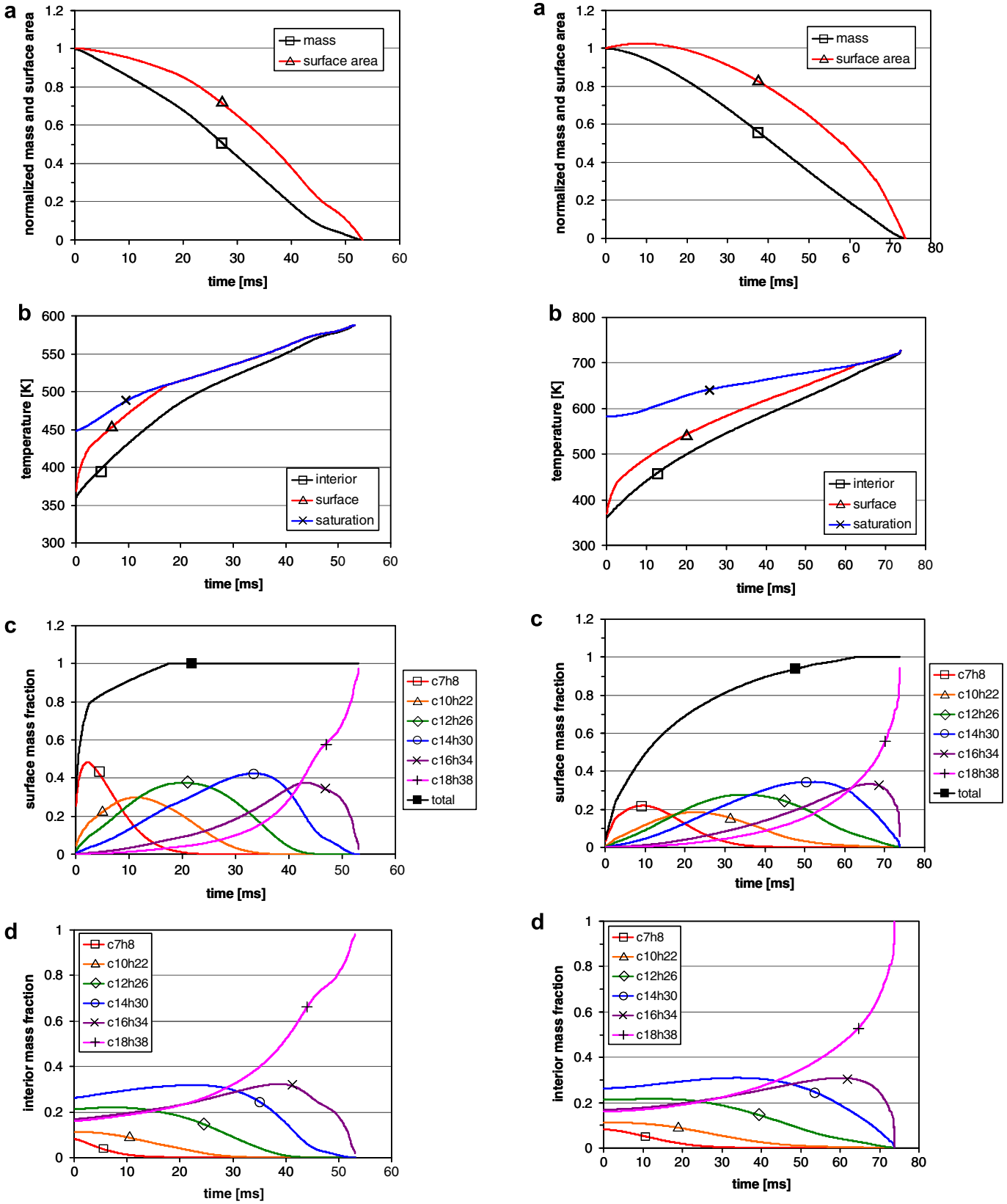

Fig. 10. Evaporation of a single diesel drop and an elevated ambient temperature. $D_o = 100$ μm and $T_{d,o} = 360$ K, $P_o = 1$ bar, $T_o = 800$ K. (a) Normalized drop mass and surface area, (b) drop interior, surface and saturation temperatures, (c) surface mass fraction of fuel components, and (d) drop interior fuel component mass fractions.

Fig. 11. Evaporation of a single diesel drop at elevated ambient pressure and temperature. $D_o = 100$ μm and $T_{d,o} = 360$ K, $P_o = 10$ bar, $T_o = 800$ K. (a) Normalized drop mass and surface area, (b) drop interior, surface and saturation temperatures, (c) surface mass fraction of fuel components, and (d) drop interior fuel component mass fractions.

the present non-reacting spray simulations. A total of 20,194 cells were employed for the sector grid. The diameter and height of the chamber were 10 and 5 cm, respectively. The resolution of the computational grid in the vertical and radial directions was uni-

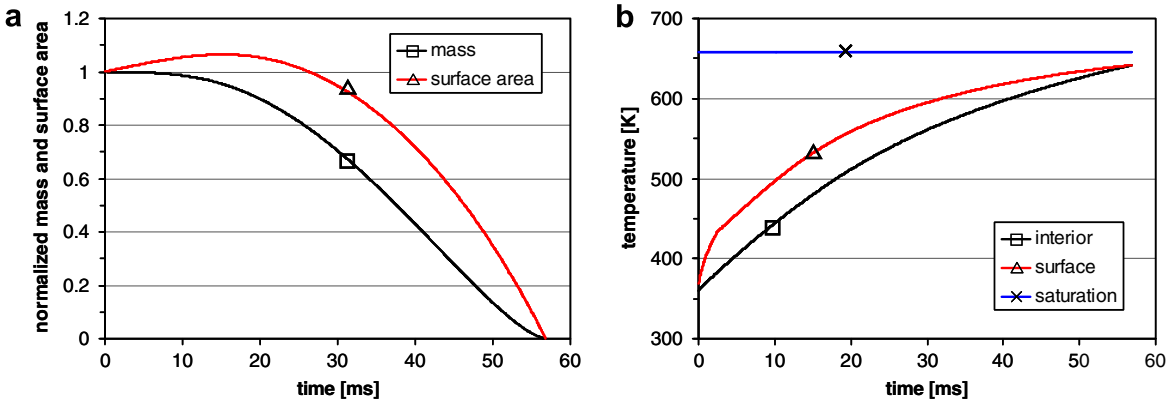

Fig. 12. Evaporation of a single tetra-decane drop at elevated ambient pressure and temperature. D_o = 100 μm and $T_{d,o}$ = 360 K, P_o = 10 bar, T_o = 800 K. (a) Normalized drop surface area and (b) drop interior, surface and saturation temperatures.

Table 2
Numerical conditions for spray evaporation simulations.

Fuel: gasoline, iso-octane	
Initial drop diameter (μm)	30
Initial fuel temperature (K)	313, 360
Ambient pressure (bar)	1
Ambient temperature (K)	500
Injection velocity (m/s)	100
Injection duration (ms)	3.0
Spray cone angle (°)	15
Fuel: diesel, tetra-decane	
Initial drop diameter (μm)	130.76
Initial fuel temperature (K)	360
Ambient pressure (bar)	30
Ambient temperature (K)	800
Injection velocity (m/s)	400
Injection duration (ms)	2.0
Spray cone angle (°)	15

form. Thirty-three cells were used in both the vertical and the radial directions, and 15 cells were used in the azimuthal direction. Injection location was 2 mm below the top surface of the chamber and 1 mm away from the axis of the chamber in the radial direction.

The same fuel compositions as those used for the single drop were used for the spray calculations. For the gasoline spray, the initial drop size was set to 30 μm, in order to decouple effects due to superheated drop conditions on the breakup process from effects on the evaporation process. The ambient air pressure and temperature were 1 bar and 500 K, respectively, and initial liquid fuel temperatures of 313 and 360 K were used. The injection velocity and duration were 100 m/s and 3.0 ms, respectively. For diesel sprays, the ambient air pressure and temperature were 30 bar and 800 K, respectively, and an effective nozzle diameter of 130.76 μm was used. The injection velocity and duration were

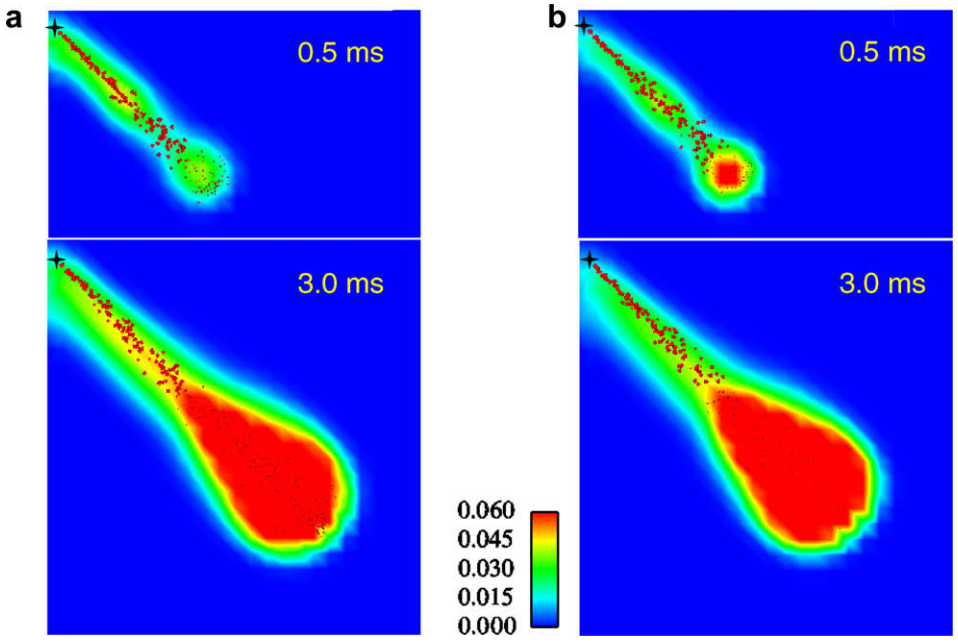

Fig. 13. Distributions of droplets and fuel mass fractions for multi-component gasoline and iso-octane spray injections in the plane of the spray. D_o = 30 μm, P_o = 1 bar and T_o = 500 K. Numbers shown in the figures are time after SOI. (a) Multi-component gasoline and (b) single component iso-octane. The injection location is 2 mm from the chamber top surface and indicated as (+) in the figures.

400 m/s and 2.0 ms, respectively. A spray cone angle of 15° was assumed for both fuels. Further details of the spray injection conditions are listed in Table 2.

In order to compare the results with one-component surrogate fuel models, the evaporation process of iso-octane and tetra-decane sprays was also simulated for the same injection conditions as in the multi-component gasoline and diesel cases.

Fig. 13 compares the droplet distributions and fuel mass fractions at two different times after the start of injection (SOI) between multi-component gasoline and single-component iso-octane sprays. The overall distributions of the spray droplets and fuel mass fractions are predicted to be similar to each other at both times. However, due to preferential vaporization of the lighter components in the gasoline case, the fuel vapor distribution becomes wider upstream of the spray plume, and more and larger droplets are seen in the region near the spray tip. The droplets in the spray tip region comprise relatively heavier components, thus it takes a longer time for the droplets to vaporize completely. The overall evaporation rate was predicted to be slightly faster in the single-component iso-octane spray case than the multi-component gasoline case.

Although the overall spray penetration and vapor mass fraction distributions look similar in the single and multi-component

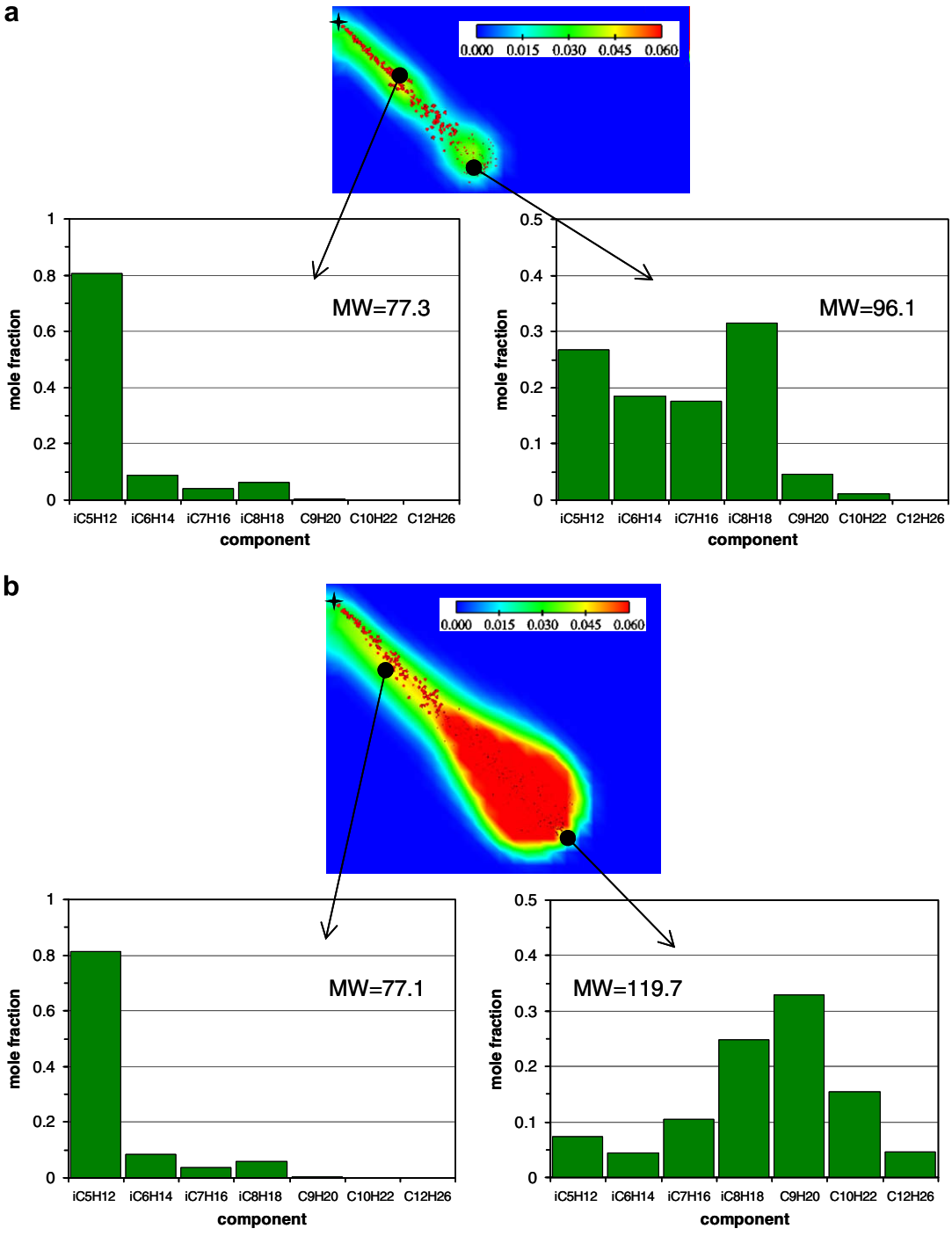

Fig. 14. Fuel component distribution of gasoline/air mixtures at various locations in the plane of the spray. Numbers in the bar-graphs are average molecular weight of fuel species at the location. Droplets are also plotted. D_o = 30 μm, P_o = 1 bar and T_o = 500 K. (a) At 0.5 ms after SOI and (b) at 3.0 ms after SOI. The injection location is 2 mm from the chamber top surface and indicated as (✦) in the figures.

cases, the local vapor fuel composition is significantly different. The distribution of fuel vapor components at various locations within the spray plume in the plane of the spray is shown in Fig. 14. At 0.5 ms, the lightest component of the model fuel composition is dominantly seen upstream of the spray plume, and thus the average molecular weight (the number in the bar-graph, 77.3 mol/g) of the fuel vapor at that location is much lower than the initial value (108.5 mol/g). On the other hand, the proportion of heavier components increases toward the spray tip, and the average molecular weight becomes closer to the initial value.

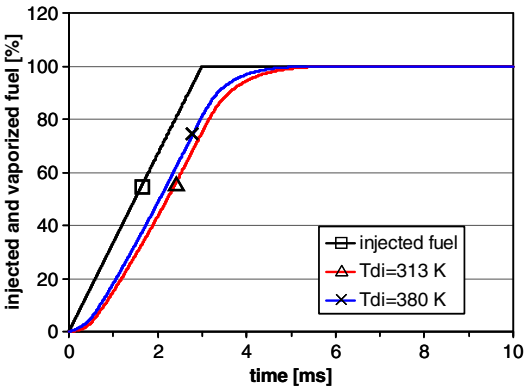

Fig. 15. Comparison of vaporized mass between normal and superheated gasoline spray injections. Injection duration was 3 ms. Fuel mass was normalized with total injected mass.

At 3.0 ms when the injection ends, the upstream average molecular weight of the fuel vapor still remains low, while the average molecular weight of fuel vapor at the spray tip exceeds the initial value due to vaporization of droplets that contain mainly the heavy-end components. It is clearly seen that the fuel vapor composition at these locations is substantially different from those upstream, as shown in Fig. 14(b). This local difference in composition, which is not accounted for in single-component fuel spray models, is expected to affect fuel/air mixing and the subsequent combustion behavior (Lippert, 1999).

In order to simulate the evaporation of superheated sprays, the initial liquid fuel temperature was raised to 380 K with all other conditions maintained the same as in the normal evaporation case shown in Fig. 13. Note that flash boiling was observed for the same initial conditions in the case of the evaporation of a stagnant single gasoline drop (see Fig. 3 in Electronic Annex 2). Fig. 15 compares the profiles of vaporized fuel mass normalized by the total injection amount between the normal and superheated spray injections. Due to the enhancement of evaporation by the superheated condition, the fuel vapor amount increases faster in the case of 380 K.

Possible effects of superheat condition and surface instability on the breakup of spray droplets and spray angle variations (Senda

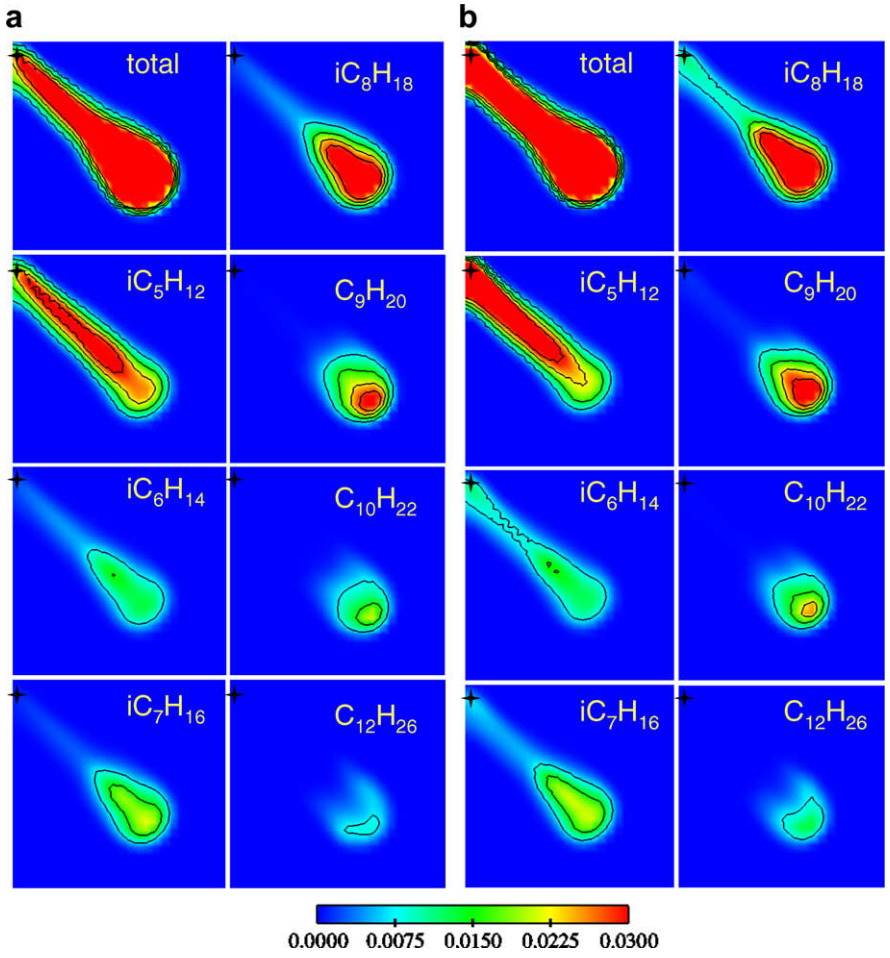

Fig. 16. Comparison of mass fraction distribution of fuel components between normal and superheated gasoline spray injections. Plots are in the plane of the spray. D_o = 30 μm, P_o = 1 bar and T_o = 500 K. Interval of iso-contours is 0.0075. (a) $T_{d,i}$ = 313 K and (b) $T_{d,i}$ = 360 K. The injection location is 2 mm from the chamber top surface and indicated as (+) in the figures.

et al., 1994; Zeng and Lee, 2007; Shusser and Weihs, 2001) were not considered in the present study. Therefore, the overall evaporation rate of the superheated spray droplets might be underestimated in the present assessment of the effect of superheat on vaporization.

In Fig. 16, the mass fraction distribution of fuel components with 380 K initial drop temperature is compared to that of the normal evaporation case. When spray droplets are injected at a superheated state, the evaporation rate is substantially enhanced through flash-boiling until the vaporization mode changes to the normal evaporation mode. Therefore, the fuel mass fraction in the near-nozzle region is increased significantly and the mass fraction iso-contour distributions become wider, as can be clearly seen from the total mass fraction distribution of the superheated gasoline injection case. Subsequently, due to the rapid decrease of drop size through evaporation, the spray droplets lose their momentum quickly, which results in shorter liquid and fuel vapor penetrations. It is expected that the superheated initial condition affects the distribution of the lighter-end components more, as can be confirmed by comparing the iC_5H_{12}, iC_6H_{14}, iC_7H_{16} and iC_8H_{18} cases in Fig. 16. Thus the flash-boiling of superheated sprays may result in more stratification of fuel components with different volatilities.

Note that the effect of superheat state on the spray cone angle variation was also not considered in the present spray model. Reitz (1990) and Senda et al. (1994) report that the spray angle is increased with increasing superheated extent. Thus, the penetration of liquid droplets and fuel vapor of the superheated sprays in the present simulations might be over-predicted since the same spray cone angles were assumed.

The present model was also applied to simulations of multi-component diesel spray evaporation. Fig. 17 compares droplet distributions and fuel vapor between multi-component diesel and tetra-decane spray injections at 0.5 and 2.0 ms after SOI in the plane of the spray. As in the gasoline case, the overall spray behavior looks similar at both times, which indicates that representing diesel fuel using a single-component surrogate fuel, which has been widely employed in diesel engine combustion research, adequately captures the overall fuel mass fraction distribution of spray injections. However, the single-component surrogate representation cannot give information about the local distribution of individual fuel components, which is important in combustion simulations, since species with different chemical structures have different chemical reaction pathways.

Local fuel component distributions at various locations and times for the multi-component diesel sprays are shown in Fig. 18. At 0.5 ms after SOI, the mole fraction distributions of the fuel components are significantly different in the areas near the injector and at the tip of the fuel vapor plume. More light components are found in the area near the injector and heavier components vaporize slower and thus are predominantly found at locations far downstream. The average molecular weights at those locations (165.0 vs. 186.6 mol/g) confirm the composition difference from the initial condition (MW = 177.1 mol/g). At 2.0 ms after SOI, similar local fuel vapor composition distributions are seen. At the tip of the spray plume the portion of heavy-end components are significantly increased, and thus the average molecular weight is higher than the initial value. This difference in the local distribution of the individual fuel components could have significant influences on spray/wall impingement too (e.g., on intake port wetting or piston impingement). The resulting wall film fuel could have a significantly different composition from the injected fuel, and this could change cold-start and/or engine emissions characteristics.

5. Summary and conclusions

A model for unsteady vaporization of multi-component sprays using the discrete multi-component (DMC) approach was presented. An explicit equation was proposed and applied to determine the heat flux from the surrounding gas to the droplet/gas interface. The equation was derived from an approximate solution of the quasi-steady energy equation. The model was implemented into a multi-dimensional CFD code and was applied to simulate evaporation processes of gasoline and diesel droplets and sprays for various ambient pressures and temperatures, and droplet temperatures. Droplet temperatures ranging from flash-boiling conditions to normal evaporation were considered. Also, the phase change processes under trans-critical conditions was modeled.

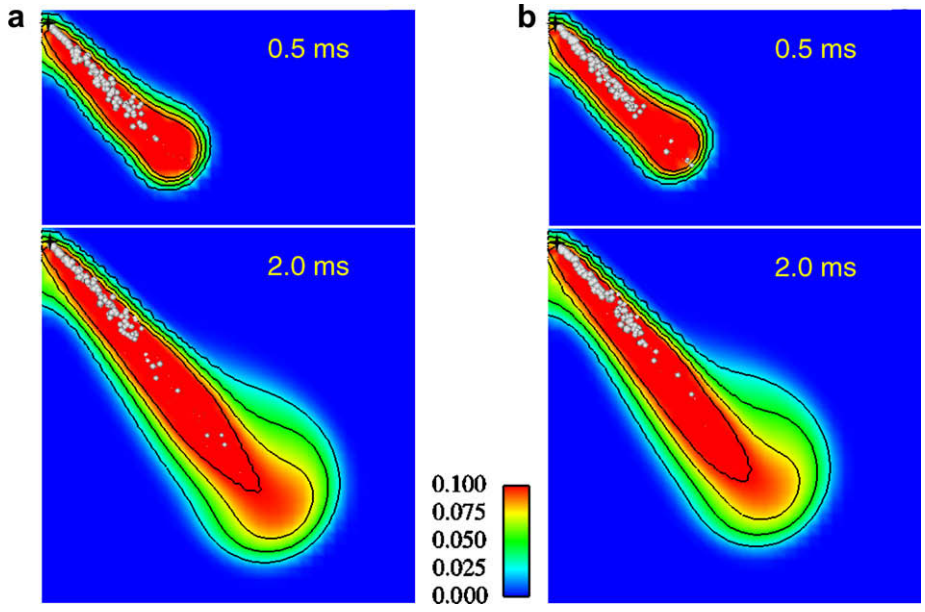

Fig. 17. Distribution of droplets and fuel mass fraction of multi-component diesel and tetra-decane spray injections in the plane of the spray. D_o = 130.76 μm, P_o = 30 bar and T_o = 750 K. Numbers shown in the figures are time after SOI. Interval of iso-contours is 0.025. (a) Multi-component diesel and (b) single component tetra-decane. The injection location is 2 mm from the chamber top surface and indicated as (+) in the figures.

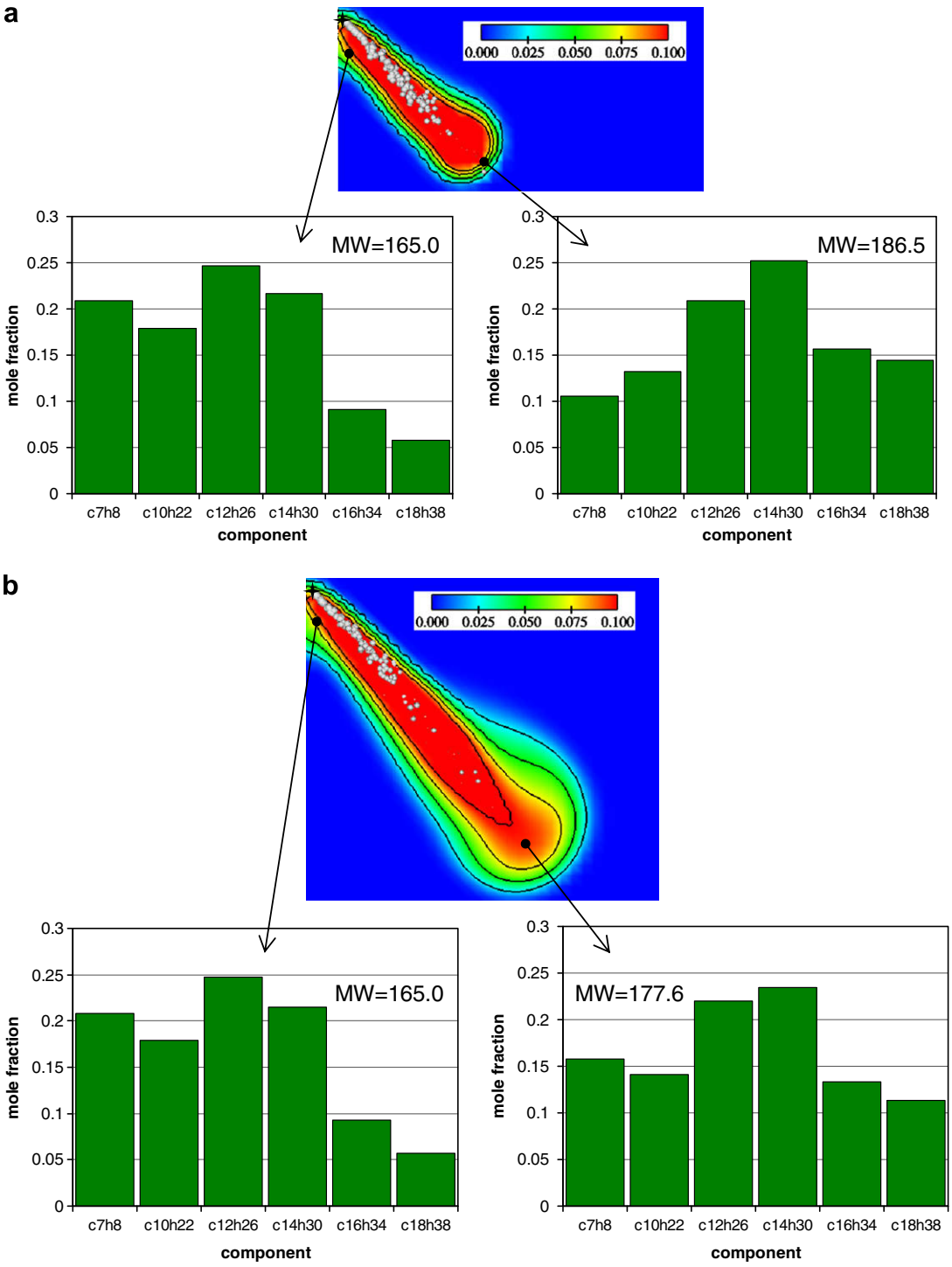

Fig. 18. Fuel component distribution of diesel/air mixtures at various locations in the plane of the spray. Numbers in the bar-graphs are average molecular weight of fuel species at the location. Interval of iso-contours is 0.025. Droplets are also plotted. D_o = 130.76 μm, P_o = 30 bar and T_o = 750 K. (a) At 0.5 ms after SOI and (b) at 2.0 ms after SOI. The injection location is 2 mm from the chamber top surface and indicated as (+) in the figures.

The evaporation of single-component surrogate fuel droplets and sprays were also calculated and compared with multi-component fuel component results. Based on the results, the following conclusions were drawn:

1. Vaporization processes of multi-component automotive fuels were successfully simulated by the present DMC evaporation model for various evaporation conditions, including super-critical and flash-boiling vaporization.
2. Multi-component single droplet evaporation differs significantly from that of a single component fuel in terms of time histories of their respective vaporization constants and droplet life times.
3. In the evaporation of single multi-component droplets, reduction of the ambient pressure not only increases the evaporation rate in the early stages of vaporization but also increases the evaporation constants during the later period of the drop life time.

4. The variation of ambient temperature is also very influential. The rate of decrease of drop life time with respect to increases in the ambient temperature decreases with increasing ambient temperature.
5. The initial drop temperature mainly affects the early stages of evaporation of single multi-component droplets. The evaporation constants during the later stages of the drop life time are independent of the initial drop temperature.
6. The present multi-component fuel vaporization model for gasoline and diesel sprays predicted similar distributions of the liquid droplets and fuel mass fractions to those from the corresponding single-component fuel. However, the local vapor fuel composition, which is not resolved by a single-component model varies significantly depending on the mixture location and times after fuel injection.
7. Preferential evaporation of the light-end components of multi-component fuels increases the amount of light-end components upstream of the spray plume. On the contrary, the heavy-end components are found predominantly in the region near the tip of the spray.
8. Flash-boiling enhances the evaporation rate of multi-component fuel sprays such that the fuel vapor distribution in the near-nozzle region becomes wider and the vapor penetration distance is shortened.

Acknowledgments

This research was sponsored by the Laboratory Directed Research and Development Program of Oak Ridge National Laboratory (ORNL) and by the Department of Energy, Sandia Labs.

Appendix A. Supplementary data

Supplementary data associated with this article can be found, in the online version, at doi:10.1016/j.ijmultiphaseflow.2008.10.006.

References

Abdel-Qadera, Z., Hallett, W.L.H., 2005. The role of liquid mixing in evaporation of complex multi-component mixtures: modelling using continuous thermodynamics. Chem. Eng. Sci. 60, 1629–1640.
Adachi, M., McDonell, V.G., Tanaka, D., Senda, J., Fujimoto, H., 1997. Characterization of fuel vapor concentration inside a flash boiling spray, SAE Paper 970871.
Amsden, A.A., 1999. KIVA-3V, Release 2, improvements to KIVA-3V, LA-UR-99-915.
Beale, J.C., Reitz, R.D., 1999. Modeling spray atomization with the Kelvin–Helmholtz/Rayleigh–Taylor hybrid model. Atomization and Sprays 9, 623–650.
Butts, R., 2008. Investigation of the effects of fuel properties on low temperature combustion in a highly dilute light duty diesel engine, M.S. Thesis, University of Wisconsin–Madison.
Carey, V.P., 1992. Liquid–Vapor Phase Change Phenomena. Hemisphere, New York.
Curtis, E.W., Ulodogan, A., Reitz, R.D., 1995. A new high pressure droplet vaporization model for diesel engine modeling, SAE Paper 952431.
Daubert, T.E., Danner, R.P., 1999. Physical and Thermodynamic Properties of Pure Chemicals: Data Compilation. Hemisphere, New York.
Davy, M.H., Williams, P.A., Anderson, R.W., 2000. Effects of fuel composition on mixture formation in a firing direct-injection spark-ignition (DISI) engine: an experimental study using Mie-scattering and planar laser-induced fluorescence (PLIF) techniques, SAE Paper 2000-01-1904.
Fuller, E.N., Ensley, K., Giddings, J.C., 1969. Diffusion of halogenated hydrocarbons in helium: the effect of structure on collision cross sections. J. Phys. Chem. 73, 3679–3685.
Givler, S.D., Abraham, J., 1996. Supercritical droplet vaporization and combustion studies. Prog. Energy Combust. Sci. 22, 1–28.
Gökalp, I., Chauveau, C., Berrekam, H., Ramos-Arroyo, N.A., 1994. Vaporization of miscible binary fuel droplets under laminar and turbulent convective conditions. Atomization Spray 4, 661–676.
Lippert, A.M., 1999. Modeling of multi-component fuels with application to sprays and simulation of diesel engine cold start, Ph.D. Thesis, University of Wisconsin–Madison.
Lippert, A.M., Reitz, R.D., 1997. Modeling of multicomponent fuels using continuous distributions with application to droplet evaporation and sprays, SAE Paper 972882.
Liu, A.B., Mather, D., Reitz, R.D., 1993. Modeling the effects of drop drag and breakup on fuel sprays, SAE Paper 930072.
Nomura, H., Ujiie, Y., Rath, H.J., Sato, J., Kono, M., 1996. Experimental study on high-pressure droplet evaporation using microgravity conditions. Proc. Combust. Inst. 26, 1267–1273.
Owen, K., Coley, T., 1995. Automotive Fuels Reference Book. Society of Automotive Engineers Inc.. p. 757.
Peng, F., Aggarwal, S.K., 1995. A review of droplet dynamics and vaporization modeling for engineering calculations. J. Eng. Gas Turb. Power 117, 453–461.
Ra, Y., Reitz, R.D., 2003. The application of a multi-component vaporization model to gasoline direct injection engines. Int. J. Engine Res. 4, 193–218.
Ra, Y., Reitz, R.D., 2004. A model for droplet vaporization for use in gasoline and HCCI engine applications. J. Eng. Gas Turb. Power 126, 422–428.
Reitz, R.D., 1990. A photographic study of flash-boiling atomization. Aerosol Sci. Technol. 12, 561–569.
Schmitz, I., Ipp, W., Leipertz, A., 2002. Flash-boiling effects on the development of gasoline direct-injection engine sprays, SAE Paper 2002-01-2661.
Senda, J., Hojyo, Y., Fujimoto, H., 1994. Modeling of atomization process in flash boiling Spray, SAE Paper 941925.
Shusser, M., Weihs, D., 2001. Stability of rapidly evaporating droplets and liquid shells. Int. J. Multiphase Flow 27, 299–345.
Sirignano, W.A., 1983. Fuel droplet vaporization and spray combustion. Prog. Energy Combust. Sci. 9, 291–322.
Smith, B.L., Bruno, T.J., 2007. Improvements in the measurement of distillation curves. 3. Application to gasoline and gasoline + methanol mixtures. Ind. Eng. Chem. Res. 46, 297–309.
Stradi, B.A., Brennecke, J.F., Kohn, J.P., Stadtherr, M.A., 2001. Reliable computation of mixture critical points. AIChE J. 47, 212–221.
Strehlow, R.A., 1985. Combustion Fundamentals. McGraw-Hill, New York. p. 64.
Tamim, J., Hallett, W.L.H., 1995. Continuous thermodynamics model for multi-component vaporization. Chem. Eng. Sci. 50, 2933–2942.
VanDerWege, B.A., 1999. The effect of fuel volatility and operating conditions on spray from pressure swirl fuel injectors, Ph.D. Thesis, MIT.
VanDerWege, B.A., Lounsberry, T.H., Hochgreb, S., 2000. Numerical modeling of fuel spray in DISI engines under early-injection operating conditions, SAE Paper 2000-01-0273.
Williams, A., 1973. Combustion of droplet of liquid fuels: a review. Combust. Flame 21, 1–31.
Williams, P.A., O'Donoghue, S., Anderson, R.W., Richardson, S.H., 2001. An experimental study of the spray characteristics of pressure-swirl atomizers for DISI combustion systems, SAE Paper 2001-01-1974.
Zeng, Y.B., Lee, C.F., 2007. Modeling droplet breakup processes under micro-explosion conditions. Proc. Combust. Inst. 31, 2185–2193.
Zhu, G.-S., Reitz, R.D., 2002. A model for high pressure vaporization of droplets of complex liquid mixtures using continuous thermodynamics. Int. J. Heat Mass Transfer 45, 495–507.
Zuo, B.F., Gomes, A.M., Rutland, C.J., 2000. Modeling of superheated fuel spray and vaporization. Int. J. Engine Res. 1, 321–336.